ELSEVIER

PII: S0032-3861(97)00162-6

Polymer Vol. 38 No. 24, pp. 6009–6022, 1997

0032-3861/97/$17.00 + 0.00

Thermally crosslinkable thermotropic copolyesters: synthesis, characterization, and processing

Patrick T. Mather*,† and Kevin P. Chaffee
Propulsion Directorate, USAF Phillips Laboratory, Edwards AFB, CA 93524-7680, USA

and Angel Romo-Uribe††
University of Southern California, Chemistry Department, Los Angeles, CA 90089-1062, USA

and Gary E. Spilman§, Tao Jiang and David C. Martin*
The University of Michigan, Materials Science and Engineering and Macromolecular Science and Engineering, University of Michigan, Ann Arbor, MI 48109-2136, USA
(Received 27 August 1996; revised 24 January 1997)

The synthesis, characterization, and processing of thermotropic copolymers composed of hydroxybenzoic acid (HBA), hydroxynaphthoic acid (HNA), and systematically varying amounts of hydroquinone (HQ) and crosslinkable terephthalic acid (XTA) are described. The XTA monomer contains a benzocyclobutene (BCB) group that lies dormant during synthesis and initial steps of processing, but that can be thermally activated to introduce covalent crosslinking between laterally adjacent macromolecules. The XTA-containing HBA/HNA copolymers all remain thermotropically liquid crystalline, and can be processed into oriented fibres by melt spinning. Rheological characterization reveals an increase in the viscosity and transition from liquid-like to solid-like behaviour as the crosslinking proceeds. X-ray diffraction reveals the changes in local organization with increasing XTA content. The microstructures of the XTA-containing copolymers (up to 20% XTA) in the condensed state are similar to those seen in HBA/HNA copolymers.

(Keywords: thermotropic; copolyesters; crosslinking)

INTRODUCTION

Thermotropic liquid crystalline polymers (TLCPs) are of scientific and technological interest because of their low melt viscosity, low shrinkage during processing, and excellent mechanical properties. TLCPs have been considered for replacing metals such as aluminium in situations where weight savings are critical to performance. However, TLCPs suffer from a number of technical limitations, including poor lateral properties, low compressive strength, high creep, low adhesion, poor flame resistance, and poor environmental stability. Also, the highly shear-thinning nature of TLCPs during melt-processing leads to heterogeneous microstructures including a thin, oriented skin, with considerably less orientation in the interior section. In order to achieve the ultimate performance of parts prepared from TLCP materials, it would be advantageous to better control the anisotropy of orientation and mechanical properties.

It has been suggested that chemical crosslinking might be one means by which current limitations in TLCP performance could be improved. Recently, a benzocyclobutene-functionalized variant of terephthalic acid (XTA) has been developed[1]. The advantages of the XTA monomer are that the benzocyclobutene (BCB) group is compact, so that upon substitution of terephthalic acid (TA) the mesophase is retained. Furthermore, the BCB group reacts only at fairly high temperatures ($T \simeq 375°C$), so that the polymer can be processed at lower temperatures, and then the reactive groups activated at a later stage in the process. Finally, the BCB group reacts without liberating small molecules that might lead to significant porosity. The known disadvantages of BCBs include a reduction in thermo-oxidative stability, and the limited availability of the monomer. Also, the influence of BCB modifications on the macroscopic properties and processing of polymers is not yet well established.

In previous work with lyotropic LCPs, we found that the incorporation of BCB groups could lead to improvements in strain to failure by kinking and reduction in creep[2]. However, it was found that kinking persisted even in highly crosslinked poly(*p*-phenylene terephthalamide) (PPTA) fibres[3]. It was proposed that one method for obtaining more uniform crosslinking across the fibre interior might be through the use of

* To whom correspondence should be addressed
† Present address: USAF Wright Laboratory, WL/MLBP, 2941 P St., Ste.1, Wright Patterson AFB, OH 45433-7750, USA
†† Present address: Systran Corp., USAF Wright Laboratory, WL/MLBP, 2941 P St., Ste.1, Wright Patterson AFB, OH 45433-7750, USA
§ Present address: GE Plastics—LEXAN Product Technology, 1 LEXAN Lane, Mt. Vernon, IN 47620, USA

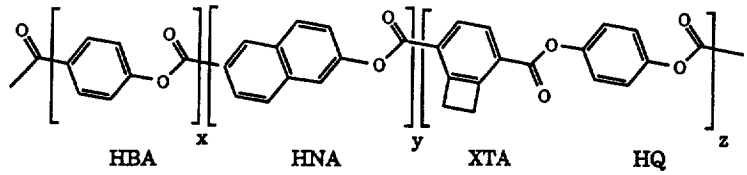

crosslinkable liquid crystalline polymers which can be processed from the melt. In this paper, we discuss the synthesis and characterization of new thermally crosslinkable thermotropic copolyesters. The copolymers investigated were based on hydroxybenzoic acid (HBA) and hydroxynaphthoic acid (HNA). We chose to examine the HBA/HNA (75/25 mol%) composition which corresponds to the commercially important Vectra™ copolymers (Hoechst Celanese Inc., Summit, NJ). To the HBA/HNA (75/25) copolymer, we incorporated systematic amounts of the crosslinkable terephthalic acid monomer (XTA) and stoichiometrically balanced equivalents of hydroquinone (HQ). The goal of this effort was to establish the existence of an accessible temperature window within which the LCPs could be processed and, if found, what composition of XTA was the most desirable.

BACKGROUND

Most thermotropic liquid crystalline polymers studied to date have been aromatic polyesters. Much of the effort has involved copolymers of hydroxybenzoic acid (HBA) and hydroxynaphthoic acid (HNA), the basis for the Vectra™ series from Hoechst–Celanese, Inc. The interested reader is referred to previous research on the synthesis[4,5], microstructure[6–12], rheology[13–20], transesterification[21,22], foaming[14], and low temperature mechanical relaxations[23] of these and similar polymers. The spinning of TLCPs into fibre has been studied by Lee *et al.*[24].

Previous research in developing crosslinkable thermotropic LCPs has included the use of epoxy functionality[25–27], in which model semiflexible LCPs are terminated with epoxy groups and the nematic melt then mixed with various diamines. A significant difference between most liquid crystalline epoxies and the crosslinkable thermotropic polymers described here is that, in the former, liquid crystallinity is induced during the polymerization and crosslinking reactions. Therefore, the nature of the liquid crystalline phase may depend on the reaction conditions. The interested reader is referred to a recent review of research in the area of liquid crystalline epoxy polymers[28].

The benzocyclobutene-functionalized terephthalic acid monomer, XTA, has now been incorporated into a number of other polymers including nylon 6,6[29], poly(benzobisthiazole) (PBZT)[30], poly(benzobisoxazole) (PBZO)[31], and poly(aryl ketones)[1]. While it has been demonstrated that BCB moieties can be efficient crosslinking agents, they have also been shown to reduce thermo-oxidative stability[2]. The opportunity to systematically examine the influence of chemical crosslinking on macroscopic properties makes the ability to control BCB concentration a useful means for obtaining fundamental new insight about the nature of liquid crystalline polymers, including insight about their mechanisms of flow behaviour.

Here, we describe the synthesis, characterization, and processing of thermotropic copolyesters that have been modified with a thermally activated BCB crosslinking agent. The capability to introduce crosslinking after the polymers have been formed into a desirable shape is expected to enable the use of these materials in demanding applications. Our hope was that this crosslinking could be accomplished without the need to significantly change well-established processing schemes.

EXPERIMENTAL

The HBA/HNA-*co*-XTA copolymers were prepared by melt polycondensation. HBA and HNA were kindly provided by Hoechst–Celanese, Inc. HQ was obtained from Aldrich Chemical Co. and used as received. The XTA was prepared with methods discussed elsewhere[1,32]. Copolymers of varying XTA content were prepared such that the mole ratio of HBA to HNA was maintained at 75/25, while mole fractions of up to 20% XTA/HQ were incorporated into the chain. Copolymer HBA/HNA-*co*-10XTA, for example, contains 90% of the HBA/HNA (75/25) mixture and 10% of a XTA/HQ (50/50) mixture. Details of the synthetic procedure have been described elsewhere[32]. Attempts to characterize the molecular weight of the polymers were unsuccessful due to insolubility in solvents commonly used for thermotropic copolyesters. In particular, pentafluorophenol was found only to swell the polymers, while mixed solvents, such as 1,1,2,2-tetrachloroethane/*p*-chlorophenol and tri-fluoro acetic acid/methylene chloride showed only minor swelling.

The synthesized HBA/HNA-*co*-0XTA copolymers were of a dusty brown colour, similar to the commercial Vectra™ materials. With the addition of XTA, the samples developed a yellow appearance similar to that of PPTA. All of the polymers were ground into powders at room temperature using a ceramic mortar and pestle, and then washed in isopropanol for approximately 15 min in order to remove any unreacted monomer or residual acetic acid from synthesis. The suspension was then filtered and dried at 125°C for 1 h in a vacuum oven.

The thermal properties of the polymers were investigated by differential scanning calorimetry (d.s.c.) using a DuPont DSC 912 (at Edwards AFB), and a Perkin-Elmer DSC-7 (at Michigan) to confirm results. Reproducible results were obtained when first scanning from 50 to 325°C at 20°C min^{-1}, then cooling to 50°C, followed by a final scan to 450°C at 10°C min^{-1}. The typical d.s.c. sample size was 10 mg. The thermal stability was examined by thermal gravimetric analysis (t.g.a.) using a DuPont TGA 951 (Edwards AFB) and a Perkin-Elmer t.g.a. (Michigan). The samples, typically weighing 25 mg, were scanned in the t.g.a. using a heating rate of 10°C min^{-1} in a nitrogen atmosphere.

The microstructure of the polymers was examined by powder wide-angle X-ray diffraction (WAXD) using a Scintag 2 kW generator with Cu–K_α fixed tube source, Ni-filtered, theta-theta diffractometer. Additionally, a

temperature-controlled stage with a tantalum heating element and a Micristar controller was used. Scans were taken at room temperature (25°C), 150°C, 250°C, 300°C, and 350°C. Powder scans were also obtained with a Rigaku X-ray generator and theta-theta symmetric reflection diffractometer. The scattering angles (2θ) ranged from 5 to 75°.

Phase identification and morphological observations of the LCPs made use of an Aus-Jena polarizing microscope and a Fluid, Inc. convective heating stage. A 25× long-working-distance objective lens was used with a 35 mm camera in conjunction with the Aus-Jena exposure system, yielding a total magnification of 250. Image analysis of fibre-swelling for assessing the state of polymer crosslinking was performed using Leitz Ortholux II and Nikon Optiphot II Pol microscopes in conjunction with a Linkam LH 1500 conductive heating stage. Images were obtained from the microscopes using a Sony CCD camera and a RasterOps frame-grabbing computer board residing in a Macintosh Quadra 700 computer running NIH Image software.

Disks of the polymers for rheological analysis were prepared from approximately 1 g of the polymer powders (25 mm diameter by approximately 1 mm thick) using a Tetrahedron compression mould at 16 MPa and 260°C for 15 min. Rheological properties were investigated using a Rheometrics RMS-605 rheometer in the parallel plate geometry for dynamic testing and in the cone-plate geometry for steady testing. Samples were heated by forced convection of dry N_2 gas, and temperature control was better than ±0.5°C.

Fibres of the HBA/HNA-*co*-5XTA and HBA/HNA-*co*-10XTA materials were prepared using a laboratory scale fibre spinning and take-up apparatus (Bradford University, Ltd.). The sample cylinder and plunger were 1.27 cm in diameter, and extrusion ram speeds of 0.5–2 mm min^{-1} were used to extrude the polymer melts through a spinneret with a diameter of 250 μm. The spinneret featured a conical contraction of 45°. The typical filament take-up speed was 20 m min^{-1}, corresponding to a nominal spin-to-stretch ratio of up to four. Fibres spun in this way were subsequently heat treated at 200°C under conditions of a nitrogen atmosphere and zero tensile loading.

Wide-angle X-ray scattering (WAXS) was used to determine the degree of preferred orientation of the fibres. A Rigaku rotating-anode generator with Ni-filtered Cu–K_α radiation ($\lambda_{Cu-K_\alpha} = 1.514$ Å) was used. The X-ray patterns were photographically recorded with a flat-plate camera; the film processing was standardized and the *d*-spacings were calibrated with silicon powder. Diffraction pattern images were digitized and subsequently analysed using Global Lab Image™ software from Data Translation, Inc. The degree of preferred orientation or order parameters $\langle P_2 \rangle$ and $\langle P_4 \rangle$ were determined by scanning azimuthally the main-interchain equatorial reflection and taking the integrated intensities along the azimuth[33]. The intensities were corrected for the background level before being analysed and the calculated values of $\langle P_2 \rangle$ and $\langle P_4 \rangle$ could be reproduced within the limits of ±0.025.

RESULTS

D.s.c. was used to determine the existence and nature of thermal transitions present in the polymers. *Figure 1a*,

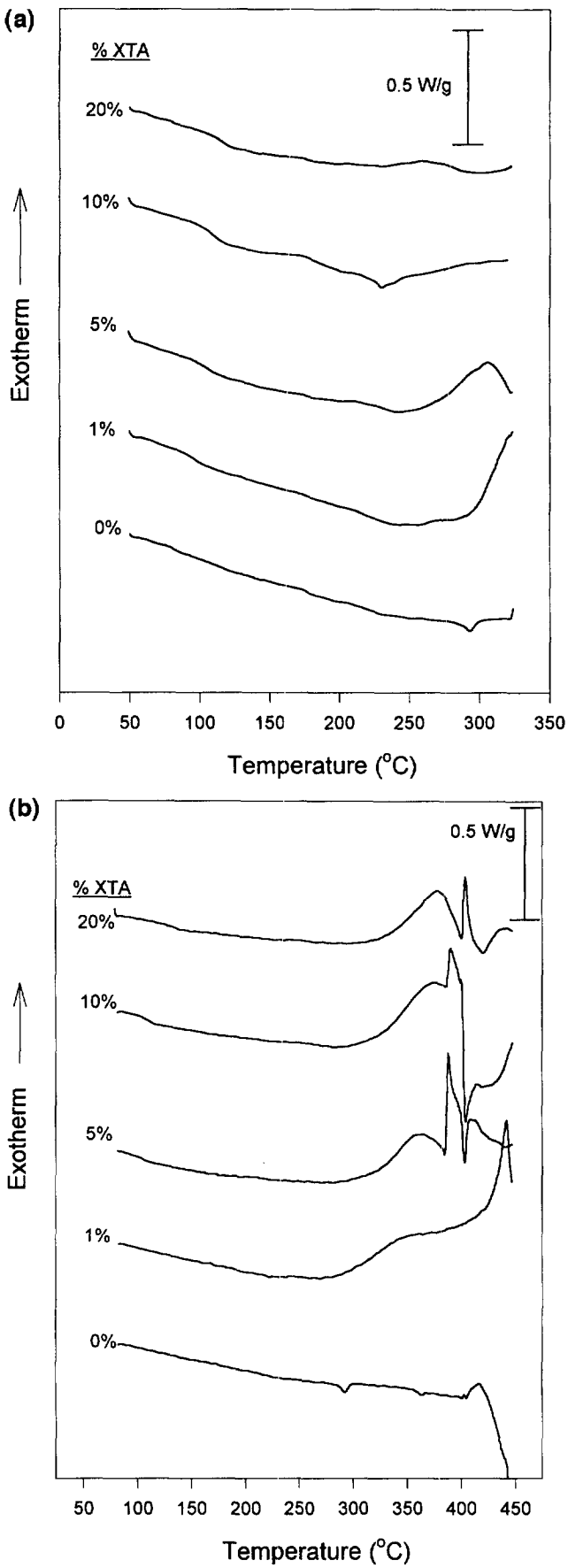

Figure 1 D.s.c. traces of the HBA/HNA and HBA/HNA-*co*-10XTA copolymers. The heating schedule involved an initial heating at 20°C min^{-1} to 325°C, followed by cooling to 40°C at 50°C min^{-1}, followed finally by a final scan to 450°C at 10°C min^{-1}. (a) First heating, (b) second heating

showing the first heating traces for a heating rate of $20°C\,min^{-1}$, displays evidence for glass transition temperatures near 100°C in all of the copolymers. It is also seen from *Figure 1a* that while the HBA/HNA-*co*-1XTA (hereafter 1XTA), 5XTA, and 20XTA samples exhibited significant exotherms (indicative of cross-linking) below 325°C, both 0XTA and 10XTA showed melting endotherms only. For 0XTA, a small endotherm is observed near 280°C, while a much more diffuse endotherm was observed for the 10XTA sample centered at 230°C. Cooling d.s.c. traces (not shown) showed no evidence of recrystallization, and displayed glass transition values similar to those seen on the initial heating.

Figure 1b shows the results of second d.s.c. heats in which the samples were heated from 75 to 430°C using a heating rate of $10°C\,min^{-1}$. For 5XTA, 10XTA, and 20XTA, well defined exothermic maxima were observed near 370°C, followed at higher temperatures by irreproducible noise evidently related to thermal degradation (see t.g.a. results below). The appearance of exothermic peaks in the reported temperature range is similar to that observed in related studies on PPTA-*co*-XTA copolymers[2]. The second d.s.c. heating of the 1XTA showed a less well defined exothermic maximum, but rather a shoulder at 350°C. Finally, the 0XTA sample showed a small melting endotherm near 290°C and a second, even smaller, endotherm at 370°C. Despite the low magnitude in the latent heat of melting at 370°C, rheological results, discussed in detail below, indicate that fluidity does not exist below this temperature. This observation is in contrast with data reported commonly on HBA/HNA (75/25) copolymers in which no second melting is observed and the material melts into the nematic state above ~295°C. We speculate that the 0XTA polymer has a comonomer sequence distribution significantly different, and perhaps more 'blocky', than the commercial HBA/HNA (75/25).

Room temperature X-ray powder diffraction data are shown in *Figure 2*. The powder diffraction pattern of the unmodified HBA/HNA copolymer is similar to that observed previously[7,10]. There is a strong peak at 4.6 Å, a medium peak at 6.5 Å, a medium peak at 3.3 Å, and a weak peak at 2.1 Å. Previous work has associated these peaks with the (110), (002), (211/210), and (006) reflections, respectively, of an orthorhombic unit cell similar to that of the HBA homopolymer ($a = 7.62$ Å, $b = 5.70$ Å, $c = 12.56$ Å)[34].

With the addition of XTA, there are a number of changes to the copolymer X-ray diffraction patterns:

1. The strong (110) peak near 4.6 Å systematically weakens in intensity and broadens in width with increasing XTA content. The peak position moves to lower angle for 1XTA, but then moves outward as the XTA content continues to increase.
2. The medium peak near 6.5 Å remains similar in intensity and width with increasing XTA content, but is missing altogether in the 10XTA material. The peak position initially moves to a higher angle, but then moves inward as the XTA content increases.
3. The (211/210) peak near 3.3 Å first sharpens and moves out to higher angle, then moves inward and fades in intensity with XTA content.
4. The (006) peak near 2.08 Å remains in nearly the same position with increasing XTA content, although it decreases in intensity and broadens somewhat.
5. The 1XTA sample shows an extra peak at 3.83 Å that is not present in any of the other samples. The intensity and width of this peak is similar to that of the (200) reflection observed in HBA/HNA.

A listing of the peak positions as a function of XTA content is provided in *Table 1*, with the *d*-spacings given in angstroms.

To complement the d.s.c. observations of melting and

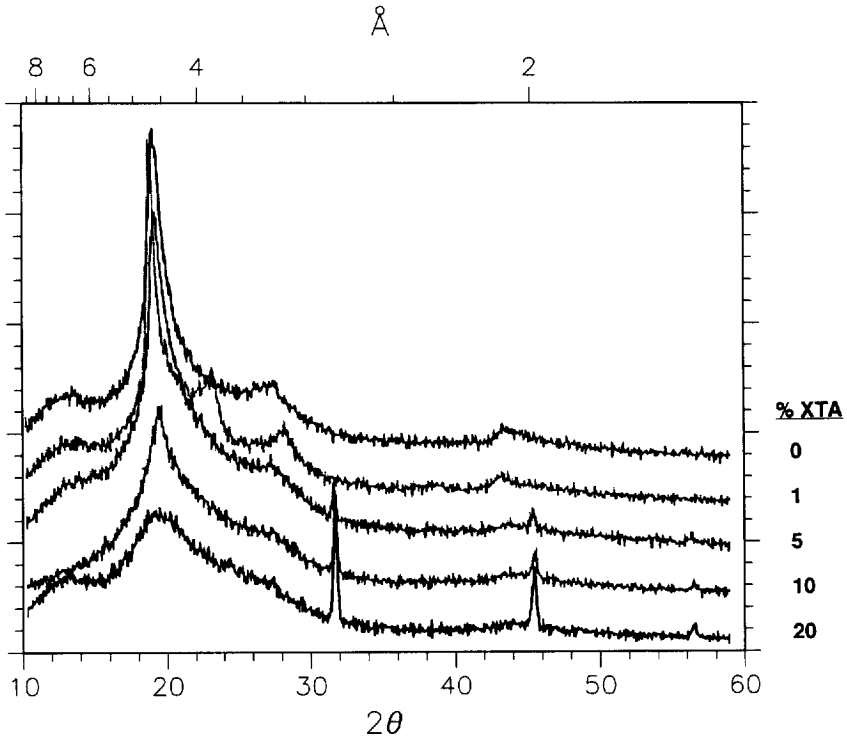

Figure 2 WAXS patterns of HBA/HNA-*co*-XTA powders as a function of XTA content

Table 1 Summary of room-temperature X-ray powder diffraction peaks[a]

Mol% XTA	Peak 1[b]: medium, stable[c], broad	Peak 2: strong, decays, widens	Peak 3: medium, only in 1XTA	Peak 4: medium, decays, broad	Peak 5: weak, decays, broad
0	6.647	4.567	–	3.308	2.078
1	6.458	4.610	3.829	3.159	2.081
5	6.539	4.549	–	3.268	2.070
10	–	4.547	–	3.271	2.070
20	6.784	–	–	3.274	2.070

[a] *d*-spacings are in Å and are accurate to ±0.005 Å
[b] Peak 1 disappears in all samples upon annealing at 125°C for several days
[c] Stable, decays and broadens all refer to trends in the peaks with increasing XTA mol%

crosslinking characteristics, X-ray diffraction patterns were gathered for all of the polymers under conditions of increasing temperature. Prior to these experiments, the samples were dried in a vacuum oven at 125°C for a period of several days. As will be seen, this thermal history had the effect of eliminating the 6.5 Å peak from the diffraction patterns. Since we will later show that the 6.5 Å peak is found on the meridian of fibre diffraction patterns of 5XTA, but not on fibre diffraction patterns of the 10XTA sample (both of which were not heat treated in the above way), it appears that the heat treatment leads to intra-chain disordering. Shown in *Figure 3a* is sequence of X-ray diffraction patterns taken on the 0XTA polymer under conditions of increasing temperature. For these experiments, the samples were thermally equilibrated at each temperature for a period of ten minutes, while the temperature was ramped between set-points at a rate of $50°C\,min^{-1}$.

On heating the 0XTA sample, both the (110) and (211/210) diffraction peaks move toward larger *d*-spacings with increasing temperature, enabling the extraction of a thermal expansion coefficient of $5.2 \pm 2.6 \times 10^{-6}\,°C^{-1}$. Additionally, for $T = 250°C$ and higher the (110) peak becomes increasingly accompanied by a broad nematic scattering peak. By 300°C, the (211, 210) peak is completely gone, and between 300 and 350°C the sample appears to have completely melted to a nematic liquid.

Figures 3b–3e show similar temperature dependence of the X-ray diffraction patterns for samples 1XTA, 5XTA, 10XTA and 20XTA, respectively, under the same conditions of increasing temperature.

The polymer samples were prepared for optical microscopy by melting the powders between glass cover slips and spreading the resulting liquid into films with thicknesses ranging from 5 to 10 μm. Polarizing microscopy of these thin films reveals fluidic birefringent textures consistent with a nematic mesophase, confirming that all of the copolymers exhibit thermotropic liquid crystallinity. Shown in *Figure 4* are example photomicrographs taken when viewing 10XTA between crossed-polarizers at 250°C before annealing (*Figure 4a*) and after annealing for 1 h at the same temperature (*Figure 4b*). A 25× objective lens was used yielding a total magnification of 250. Prior to annealing (*Figure 4a*), the sample displays a mottled, birefringent morphology characterized by regions of distinct 'director' orientation separated from one another over an average length scale of 1 to 10 μm. Here the term 'director' refers to the direction of preferred molecular orientation. The observed spatial variation in direction orientation is possibly accommodated by singular disclination lines or walls[35], but not necessarily so. Our limited resolving power is not capable of unambiguously identifying disclination lines or walls within the observed morphologies and transmission electron microscopy (TEM) observations would be useful.

Superposed on the fine microstructure (1–10 μm) is a morphology of a large length-scale over which intensity (retardation) fluctuates. On annealing (*Figure 4b*), this morphology gives way to one featuring regions of homeotropic director alignment—director perpendicular to the plane of the film—spanning large areas of the sample (25–100 μm). That these regions were homeotropic was confirmed by lightly shearing the film and observing transmission of light through regions which were formerly homeotropic. Further annealing at 250°C did not lead to homeotropic alignment of the entire sample, possibly due to inhomogeneities on the glass surfaces. Annealing had the additional effect of coarsening the smaller length-scale microstructure within the non-homeotropic regions by about a factor of two.

Optical microscopy studies further support the conjecture that it is the onset of the BCB-crosslinking reaction that leads to the exotherm above 350°C observed in the d.s.c. traces. When fibres of the copolymers have been heated through this temperature range, subsequent exposure to pentafluorophenol (PFP), a solvent for the HBA/HNA polymer, leads to swelling which systematically decreases with the temperature of annealing. *Figure 5* shows the amount of room-temperature PFP-induced swelling observed for 10XTA sample as a function of annealing temperature. Here, we quantify the swelling behaviour by determining the ratio of the fibre diameter after and before PFP exposure. It is seen that the swelling decreases as the annealing temperature increases.

Also shown in *Figure 5* are data addressing the reversibility of the solvent swelling. The lower curve shows the final diameter of the swollen fibre after the temperature was raised to 450°C, driving off the residual solvent. For samples heat treated above 330°C, the swelling is essentially reversible, with the final shape after solvent liberation being essentially the same as that of the original sample. However, when the samples heat-treated at temperatures below 330°C were swollen, a degree of this strain was irreversible, evidently indicating that a permanent crosslinked network had not yet been established.

T.g.a. scans indicate that the onset of thermal degradation occurs at temperatures decreasing with increasing XTA content, as shown in *Figure 6*, from 440°C for 0XTA to 400°C for 20XTA. Additionally, the amount of residual char seen at elevated temperatures was less dependent on XTA content than degradation onset. In particular, the residual char content observed at 900°C was roughly 40% for all of the polymers and was highest for 0XTA with a value of 42%. The decrease in thermal stability with XTA content at temperatures near 400°C was also seen as an increase in the amount of blackening and discolouration of 10 ml glass vials containing equivalent amount of the various copolymers during heating at 400°C in a furnace flushed with nitrogen.

All of the XTA copolymers were characterized using melt rheology techniques to complement the thermal characterization results (d.s.c. and X-ray diffraction)

and to establish a processing temperature window within which the polymers would be most easily moulded or spun into fibres. Since the crosslinking reaction is kinetically controlled, it is necessary to determine the rate of this reaction to establish the constraints on processability. With these goals in mind, we chose to perform dynamic oscillatory measurements under conditions of increasing temperature and isothermal dwells. For temperature sweeps, a heating rate of $5°C\,min^{-1}$ was used. Strain amplitudes were set initially at 1% and adjusted during the test to maintain linearity in the rheological material functions. For the crosslinking samples, temperature sweeps were complicated by the fact that expansion of the rheometer tools during heating could not be accommodated by outflow of material (as is usual for polymer melts) and led to a large normal force. Once the normal force exceeded 500 g, the test was terminated. It was also possible to conduct a manual temperature sweep by raising the top fixture in direct compensation for the thermal expansion.

Figure 7 shows the temperature dependence of the dynamic viscosity. The 0XTA (HBA/HNA (75/25)) copolymer does not melt completely until $T \simeq 370°C$, at which point the dynamic viscosity falls precipitously. This is in contrast to the HBA/HNA (75/25) copolymer reported in the literature to have a melting point of $\simeq 295°C$. Possible explanations for this apparent discrepancy include a large dependence of melting point on copolymer composition, and a sensitivity of TLCP phase behaviour to variations in the HBA/HNA sequence distribution along the chain[36]. Additionally, the high melting transition we observe with rheological measurements is higher than that measured with the controlled-temperature XRD patterns ($300°C < T_m < 350°C$, *Figure*

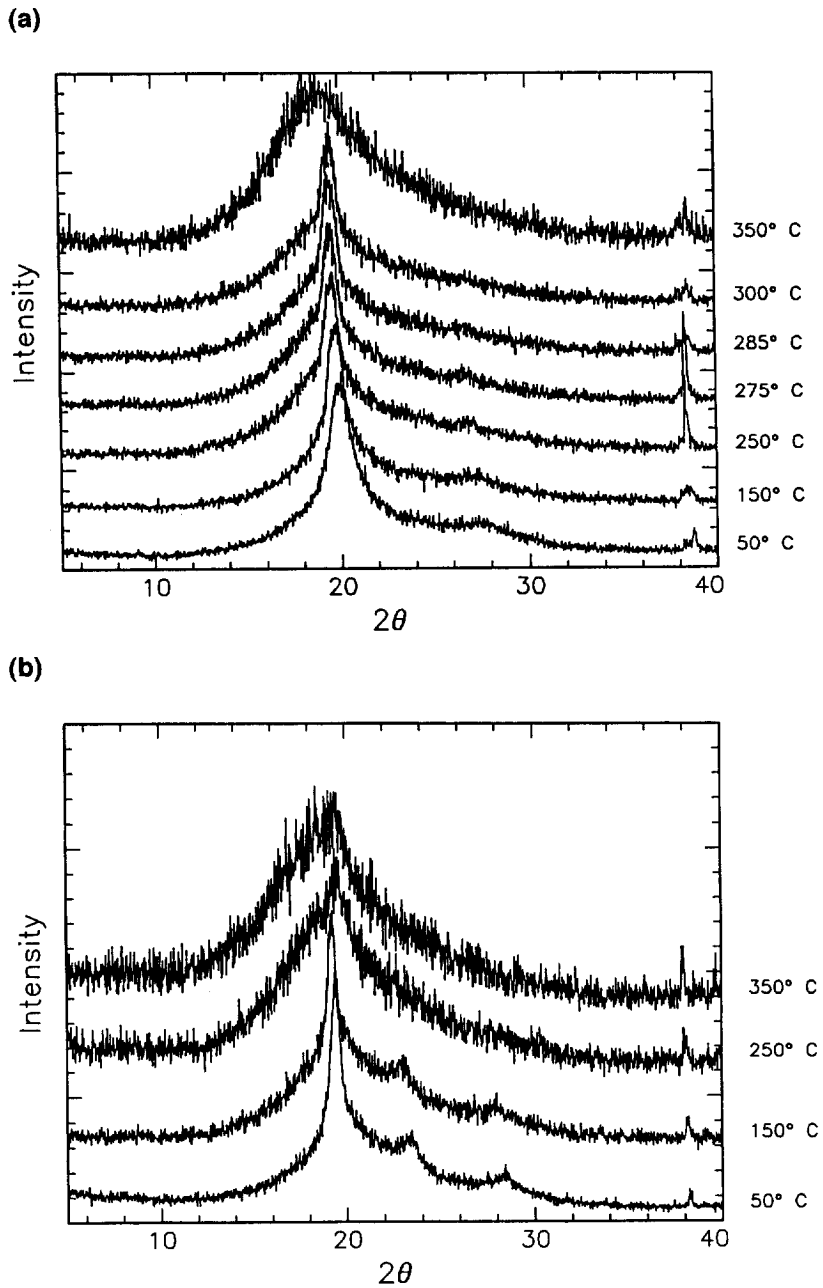

Figure 3 Powder WAXS patterns for (a) 0XTA, (b) 1XTA, (c) 5XTA, (d) 10XTA, and (e) 20XTA polymers as functions of temperature showing the melting behaviour of the copolymers

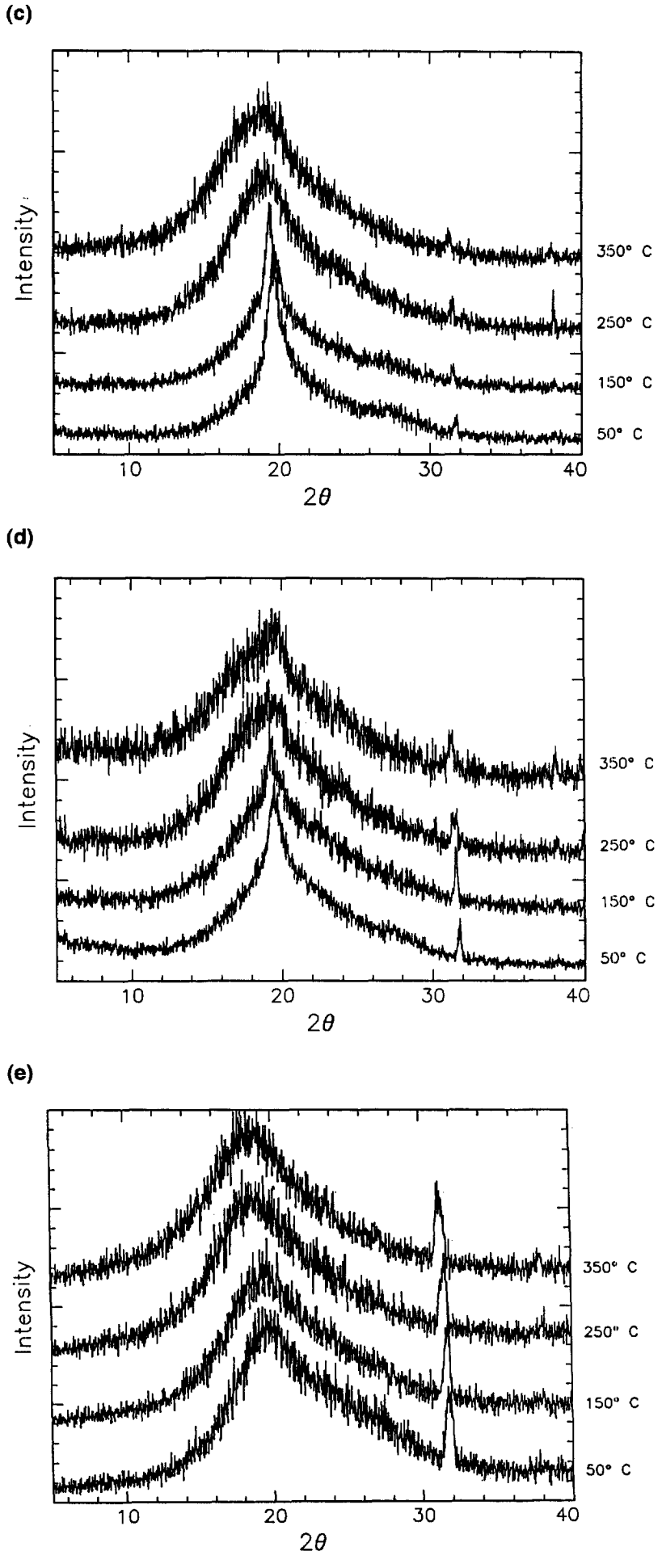

Figure 3 Continued

3a). We attribute this difference in observed melting point to the substantial difference in heating rates between the XRD ($50°C\,min^{-1}$) and rheology ($5°C\,min^{-1}$) experiments.

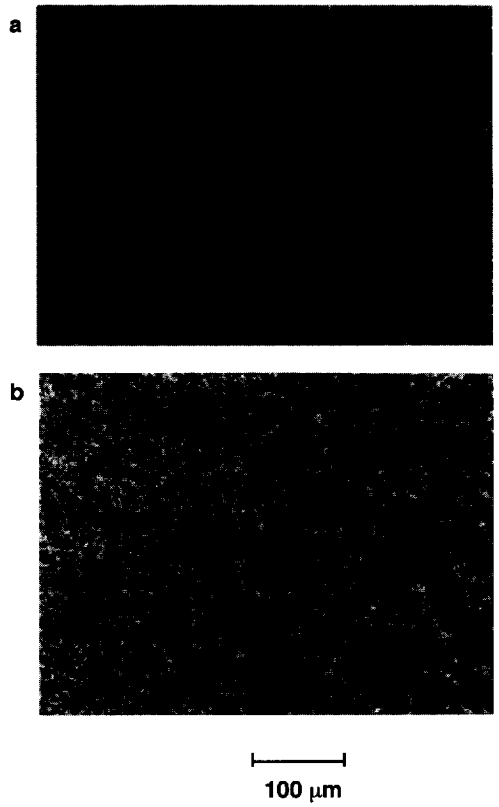

Figure 4 Polarizing optical microscopy (POM) of 10XTA in the nematic state at 250°C before annealing (a) and after annealing for 1 h (b). On annealing, large regions of the mottled birefringent texture become homeotropically oriented, appearing black between the crossed-polarizers

Once the temperature of the 0XTA sample reaches about 390°C, however, the dynamic viscosity stops decreasing and remains virtually unchanged up to 400°C. To test the possibility that this sample was also crosslinking, perhaps via a Fries reaction[22], the dynamic viscosity was monitored for an extended period of time at 400°C. The results are shown in *Figure 8*, where it is seen that despite an order of magnitude rise in dynamic viscosity over a period of approximately 20 min, the mechanical spectrum (shown as inset) at the end of this period indicated that the polymer had not crosslinked, but had instead chain-extended via transesterification to a sample of increased molecular weight. This observation was corroborated by the visual observation that during the isothermal annealing at 400°C the sample edges protruded increasingly (although less than 5% of the disc radius) with time in a manner consistent with foaming resulting from acetic acid evolution during the chain-extension process.

Also shown in *Figure 7* are the XTA-containing copolymer temperature sweeps. The 1XTA copolymer shows no clear melting transition, although the dynamic viscosity begins to decrease significantly at 280°C and shows a viscosity minimum (although still large at 2×10^6 Poise) at 318°C. The loss tangent ($\tan\delta = G''/G'$) is less than 1 ($\simeq 0.5$) for almost the entire temperature sweep, indicating elastic-dominated rheological behaviour. The 5XTA copolymer exhibits the same qualitative behaviour as the 1XTA sample, with a slightly lower viscosity minimum ($\simeq 10^5$ Poise) which occurs at a lower temperature of 300°C. In comparison, the 10XTA copolymer behaves quite differently. The viscosity decreases gradually from the temperature at which the sample is loaded into the rheometer (200°C) and shows a relatively low viscosity minimum of 1500 poise at about 320°C accompanied by a large loss tangent (>2). On continued heating the viscosity increases rapidly. Above 350°C, the dynamic viscosity

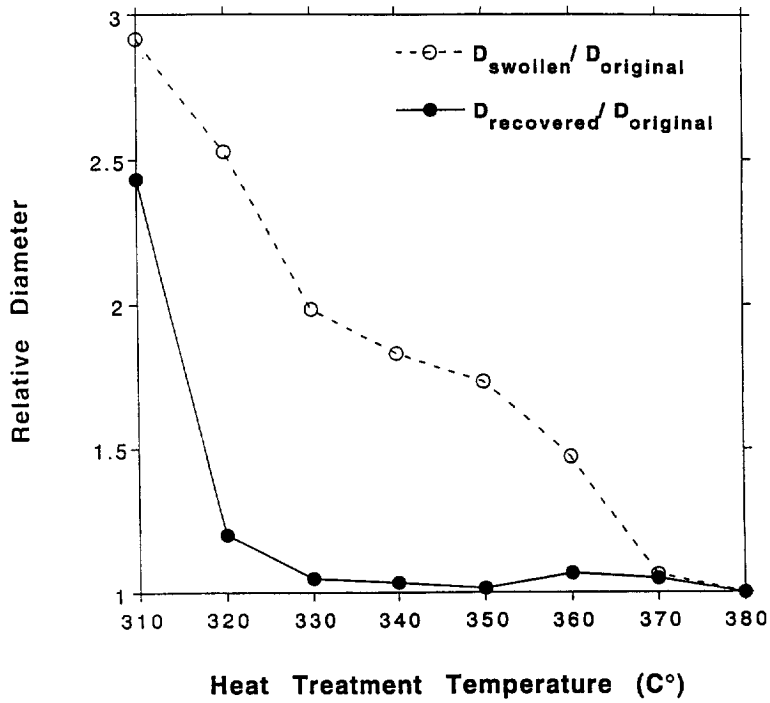

Figure 5 Change of the diameter of the HBA/HNA-*co*-10XTA copolymer fibres during swelling in pentachlorophenol, following heat treatments at various temperatures. As the annealing temperature increases, the amount of solvent swelling decreases

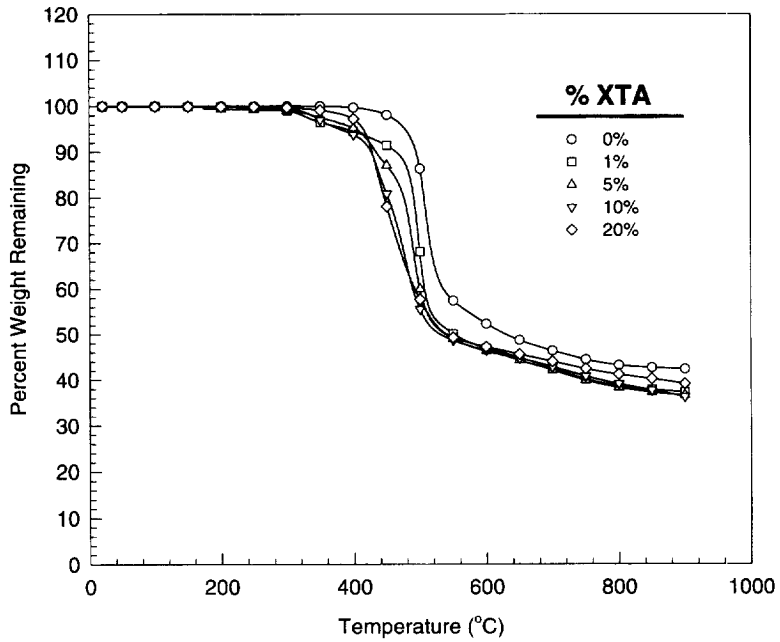

Figure 6 T.g.a. traces of the HBA/HNA-*co*-XTA copolymers as a function of XTA content. The XTA-containing copolymers are less thermally stable near 400°C, but show improved char formation above 800°C

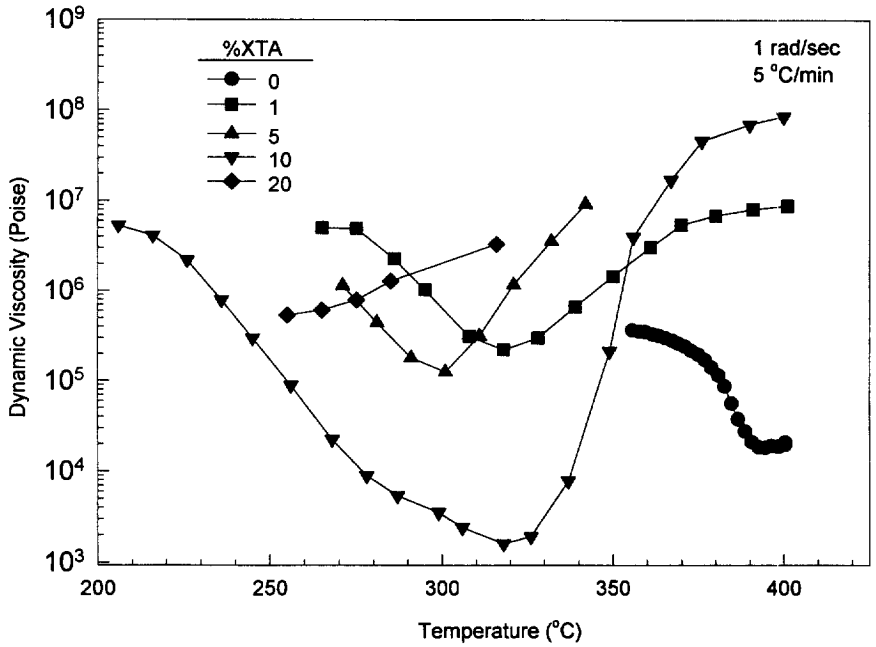

Figure 7 Dynamic viscosity of the HBA/HNA-*co*-XTA copolymers as a function of temperature for various levels of XTA content. The minimum viscosity occurs at a lower temperature with increasing XTA content. Oscillation frequency is 1 rad s^{-1}, strain amplitude is 1%, and the heating rate is 5°C min^{-1}

($|\eta^*|$) becomes larger than 10^7 dyn cm^{-2} at which point transducer-compliance effects become significant. The HBA/HNA-*co*-20XTA polymer showed viscosity increasing with temperature from the moment the temperature sweep was started at 255°C, suggesting that the cross-linking reaction had started before polymer had melted.

While the 10XTA copolymer showed promising rheological results for ease of processability, it was necessary to monitor the time evolution of rheological properties under isothermal conditions for temperatures at or near the viscosity minimum to establish the cross-linking kinetics under conditions required for processing operations such as fibre spinning or extrusion. Three isothermal temperatures were investigated: 255, 275 and 298°C. For each experiment, a 10XTA sample disk (1 mm in thickness) was loaded into the rheometer at the test temperature, the rheometer fixtures having been allowed to thermally equilibrate for a period of 30 min. Once the samples were loaded, data collection began following a 2-min delay to allow the temperature of the sample to reach that of the plates.

Shown in *Figure 9* is a plot of the storage modulus, G', loss modulus, G'', and complex viscosity, $|\eta^*|$, as functions of time at 255°C using an oscillation frequency

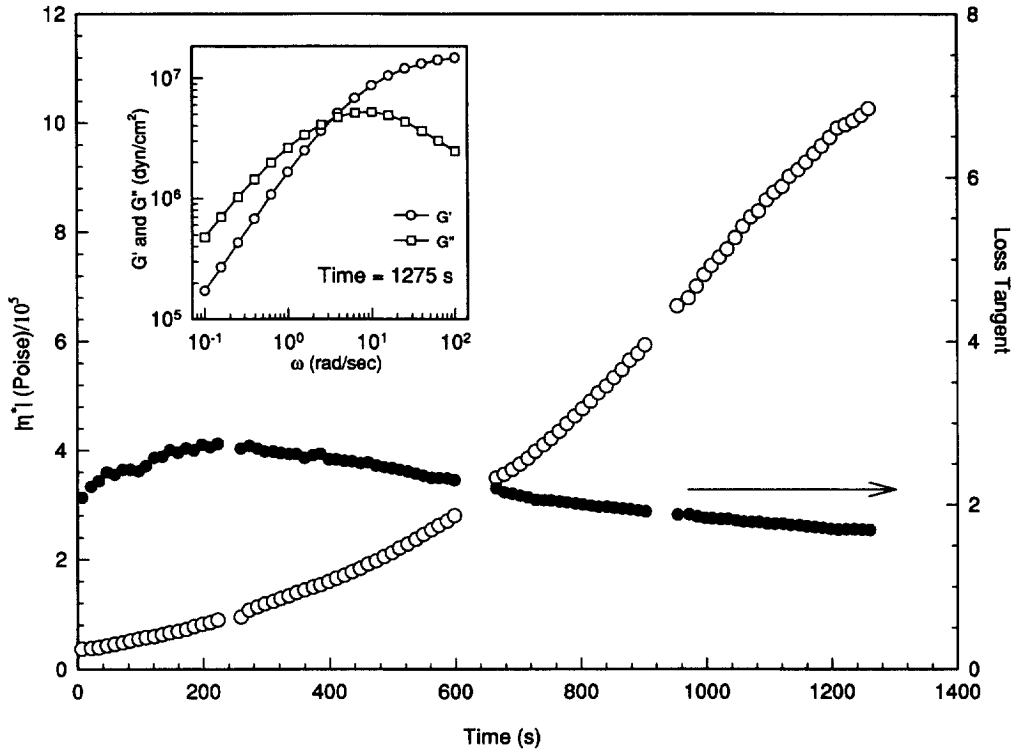

Figure 8 Dynamic viscosity of the 0XTA sample at 400°C showing a dramatic increase in viscosity with time. Frequency is 1 rad s^{-1} and amplitude is 1%. Shown as inset is a dynamic mechanical spectrum indicating that the sample has not crosslinked, but rather has increased viscosity by linear molecular weight enhancement

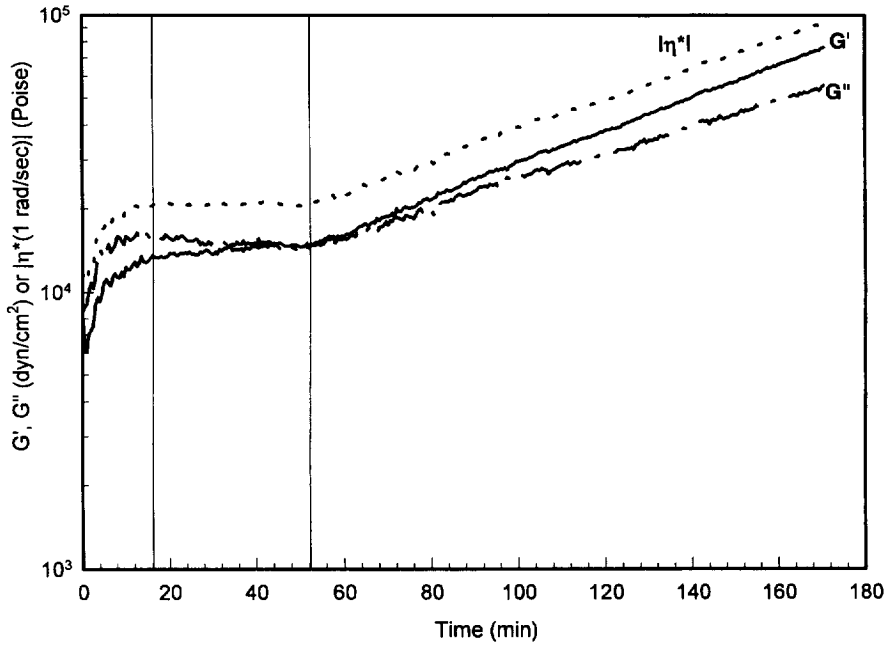

Figure 9 Plot of storage modulus, G', loss modulus, G'', and dynamic viscosity $|\eta^*|$, as functions of time at 255°C for HBA/HNA-*co*-10XTA. Oscillation frequency is 1 rad s^{-1}, and strain amplitude is 1%

of 1 rad s^{-1} and a strain amplitude of 5%. Three time zones are clearly seen. First, the viscosity increases two-fold when first loaded in the rheometer, possibly due to an increase in molecular weight. After this initial viscosity increase, a period of 30 min transpires in which the rheological properties remain unchanged. Following this period of constant rheological properties, the moduli begin to increase exponentially. Coinciding with the onset of an exponential increase in viscosity is the crossing of G' with G'', suggesting the possibility that the material has undergone a transition through a gel point[37], although it was not confirmed that the loss tangent became independent of frequency, a more rigorous test for gelation, at the same point in time. The exponential increase in dynamic moduli indicates the kinetics of crosslinking are similar to those seen in thermosetting flexible polymers[38] and other thermosetting LCPs[28].

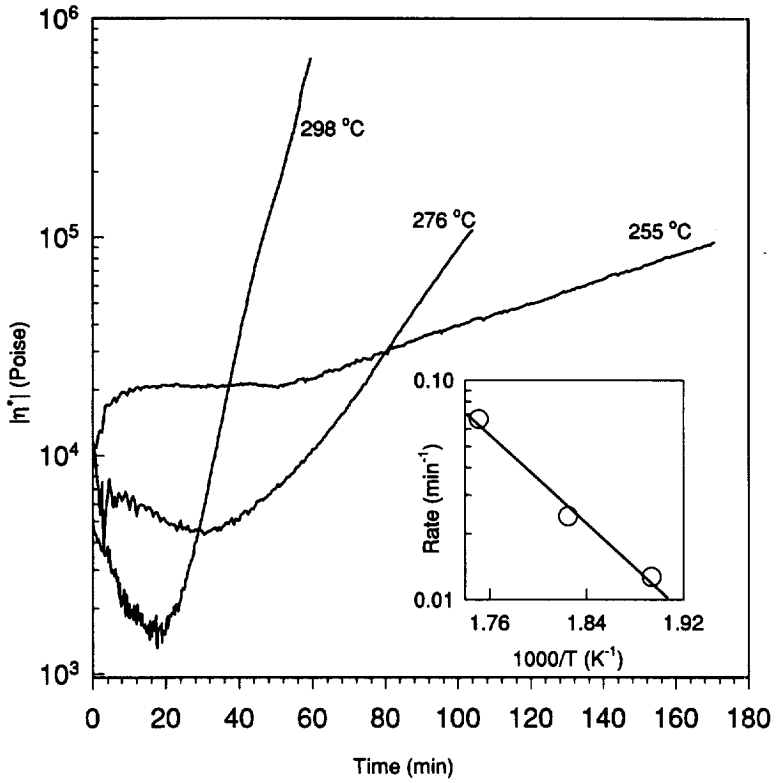

Figure 10 Plot of the dynamic viscosity HBA/HNA-*co*-10XTA as a function of time at various temperatures. Oscillation frequency is 1 rad s^{-1}, strain amplitude is 10%. Inset shows an Arrhenius plot used to determine the activation energy, E_a, of the crosslinking reaction

The rate of crosslinking was found to depend strongly on temperature. *Figure 10* is a plot of the dynamic viscosity monitored during isothermal crosslinking, where it is seen that several distinct changes occur with increasing crosslinking temperature. First, of great practical interest is the decrease in incubation time with increasing temperature. This time is reduced from nearly 50 min for $T = 255°C$ to less than 20 min for $T = 298°C$. The crosslinking reactions were terminated prior to completion, as the torque signals became too large for the strain amplitude used (which needed to be high enough for meaningful low viscosity data). We analysed the curves in *Figure 10* by fitting the straight portions of the curves on the log-linear plot to reveal the reaction rate, α, from the fitting equation, $|\eta^*| = |\eta_0^*|\exp(\alpha \cdot (t - t_0))$. A plot of $\log \alpha$ vs $1/T$ (shown as the inset of *Figure 10*) made possible the determination of an apparent activation energy, E_a, in the expression $\alpha = \alpha_0 \exp(-E_a/RT)$. The apparent activation energy obtained from this analysis is $99 \pm 6\,kJ\,mol^{-1}$. This number compares reasonably well with values of the heat of reaction of BCB model compounds (ranging from 40 to 208 kJ mol^{-1}, typically 82 kJ mol^{-1}) as reported by Deeter *et al.*[39]. The measured activation energy is also similar to the value of the heat of polymerization of 105 kJ mol^{-1} found in BCB-functionalized compounds with no reactive unsaturation[40].

Given the large incubation time of the 10XTA copolymer at 255°C, we were able to evaluate the steady shearing-flow behaviour of the uncrosslinked thermotropic melt over a range of shear rates. For this test, the cone-plate geometry was used with 25 mm diameter fixtures and a cone angle of 0.04 rad. The shear rate was increased from 0.01 s^{-1} to approximately 40 s^{-1} at which point fracture of the sample-edge became significant. The results, shown in *Figure 11*, reveal strong shear thinning behaviour for the entire range of shear rates investigated, with a power-law slope near −0.5, similar to the region I viscosity scaling first identified by Onogi and Asada[41], in lyotropic LCPs and to data on TLCPs reported by Kalika *et al.*[14]. This behaviour appears to be a general characteristic of LCP rheology and is often discussed in terms of disclination-mediated mechanisms of flow[42].

During rheological characterization, we observed some evidence of foaming of the polymers at high temperatures, despite our efforts at minimizing this effect through heat treatment and drying. The observed foaming was probably the result of transesterification reactions of the chain ends leading to liberation of acetic acid, and suggests that the polymers are of initially low molecular weight. Despite these observations, no significant mass loss was seen at similar temperatures in the t.g.a. The discrepancy may be due to the fact that during the 20°C min^{-1} temperature sweep in the t.g.a. the viscosity is increasing rapidly enough due to crosslinking that any evolved acetic acid remains trapped in the material. Such behaviour suggests possibilities for high modulus structural foams using these materials with low starting molecular weights (high concentration of end groups). During the isothermal rheological testing of 10XTA, the extent of foaming was seen to increase over the same range in which BCBs could react. Some foaming was also seen in the 0XTA sample, containing no BCB, suggesting that it is not coupled to a reaction involving this moiety. Future efforts will focus on end-capping the polymers following synthesis to impede the liberation of small molecules at elevated temperatures.

The thermal and rheological characterizations indicate that there is a temperature window for the HBA/

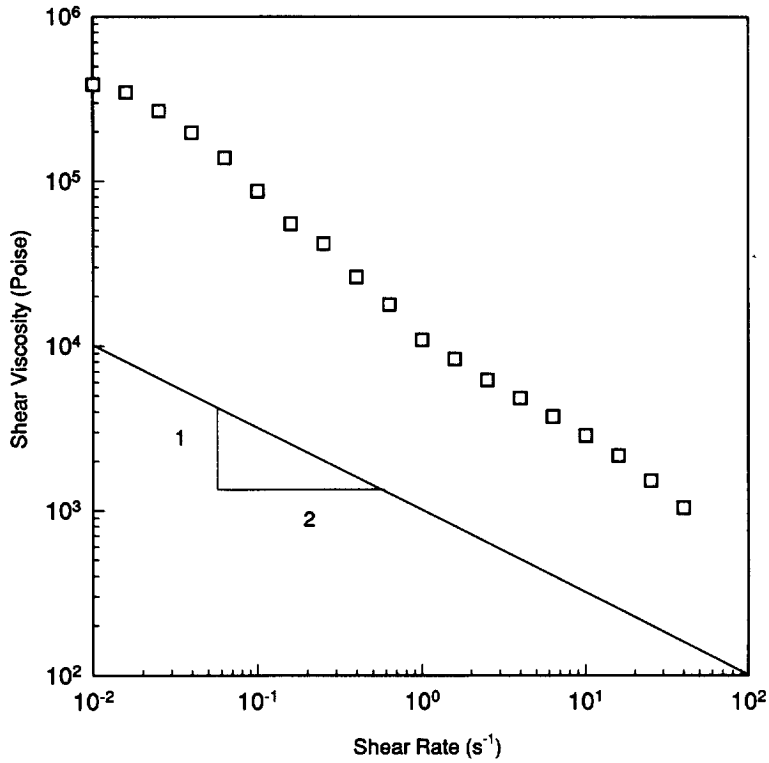

Figure 11 Steady shear viscosity vs shear rate for the 10XTA copolymer measured using a cone-plate rheometer at 255°C. The data were obtained with shear rate increasing using a cone angle of 0.04 rad and a sample diameter of 25 mm

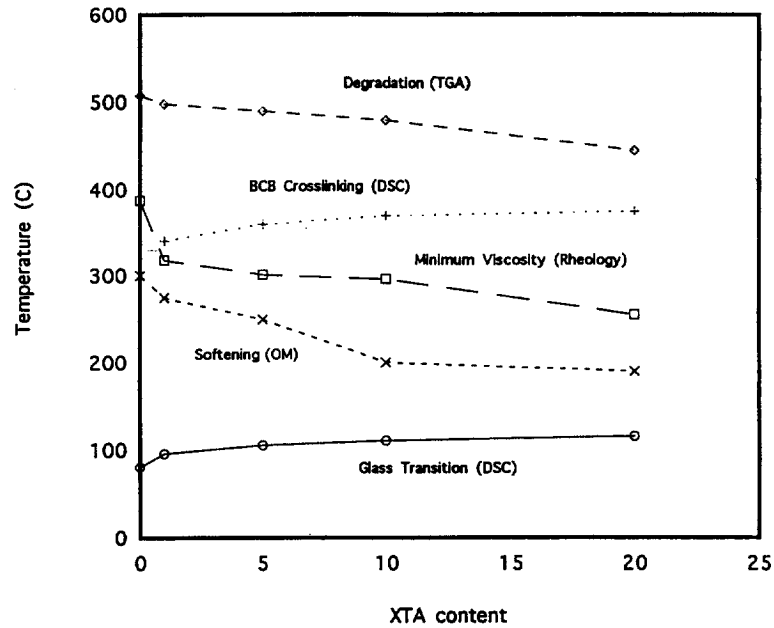

Figure 12 Characteristic temperatures as a function of XTA content. The glass transition (d.s.c., Perkin-Elmer and DuPont) increases slightly with XTA content. The softening temperature was determined by hot stage optical microscopy (Linkham, Leitz), and decreases with XTA content. The minimum viscosity data were obtained by rheology (Rheometrics), and decreases with XTA content. The crosslinking temperature was determined by d.s.c., and increases with XTA content. The degradation temperature was determined by t.g.a. and decreases with XTA content

HNA-*co*-XTA polymers within which melt processing is possible. A comparison of the various characteristic temperatures are shown in *Figure 12* including the glass transition (d.s.c.), softening (OM), minimum viscosity (rheology), crosslinking exotherm (d.s.c.), and thermal degradation (t.g.a.) temperatures. The minimum viscosity occurs above the glass transition and softening temperature but below the crosslinking exotherm. Note that the glass transition temperature (T_g) and crosslinking exotherm temperatures both increase slightly with XTA content, while the softening, viscosity minimum, and onset of thermal degradation temperatures all decrease with additional XTA. To process these crosslinkable TLCPs, time-monitoring and temperature control are critical, because the reaction can continue to lead to curing in the processing equipment. The curable

nature of these LCPs provides an additional means for controlling their macroscopic properties. Further work will be necessary to address the impact of this cross-linking on properties of specific interest for a given application.

Fibres spun from copolymers 5XTA and 10XTA using a laboratory scale fibre spinning apparatus (Bradford University, Ltd) were examined using XRD. The fibre WAXS patterns are shown in *Figure 13* for filaments melt spun from the 5XTA and 10XTA copolymers. It is clear that the molecules in the copolymer filaments are oriented, although the degree of structural perfection is less well developed than in typical solution spun PPTA, PBZO, or PBZT fibres. It is also clear that the 5XTA sample is substantially more crystalline than the 10XTA sample. The two factors most likely contributing to this comparatively low level of orientation are: (1) the molecular weights of the polymers are likely low; (2) the large number of comonomers may lead to substantial disorder in the sequence distribution along the chain which should minimize interchain registry on solidification. There are three discrete reflections observed on the equator, and these increase in intensity and sharpness after heat treatment at 200°C. There are also three distinct reflections on the meridian. The fibre patterns also reveal that certain sharp reflections which were originally observed in powder WAXS were related to crystalline particles present in the polymer as a by-product of the synthesis, and were not representative of the copolymer morphology itself.

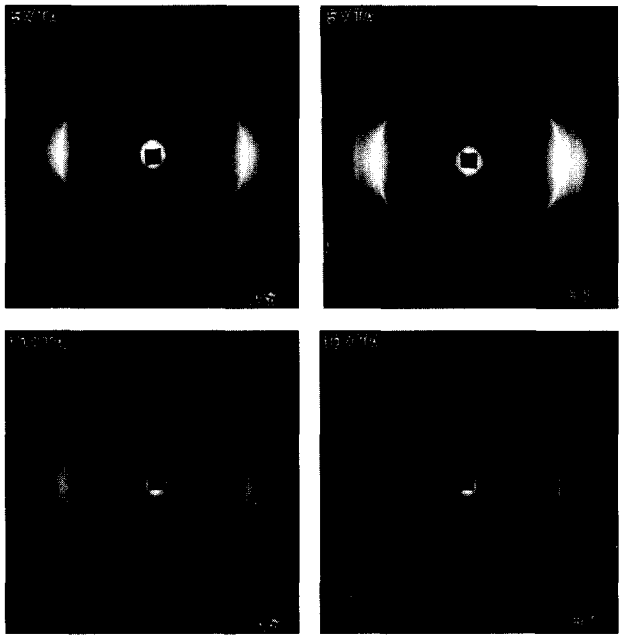

Figure 13 Fibre WAXS patterns of HBA/HNA-*co*-5XTA and HBA/HNA-*co*-10XTA as-spun (AS) and heat treated at 200°C under zero load for 2 h. The primary equatorial reflection occurs at $2\theta = 19.5°$

The diffraction patterns show that the as-spun fibres crystallize as a pseudo-hexagonal (PH) structure where the main peaks are the prominent (110) equatorial and (211) (*Figures 13a* and *13b*). Note that the 5XTA fibre shows a broad meridional (002) reflection, and higher degree of crystallinity, evidenced by the sharp equatorials. On annealing, the equatorial reflections sharpen (in 2θ), indicating an increase of crystallinity in both samples (*Figures 13c* and *13d*). In addition, during the crystallization process the 5XTA fibres transform to a orthorhombic phase[8], which is characterized by the presence of a (200) equatorial peak in addition to the intense (110). The degree of preferred orientation, quantified by the parameters $\langle P_2 \rangle$ and $\langle P_4 \rangle$, was determined by scanning azimuthally the main-interchain equatorial maximum of the patterns of *Figure 13*. *Figure 14* shows a plot of integrated intensities as a function of azimuthal

Table 2 Summary of measured orientation parameters for as-spun (AS) and heat-treated (HT) XTA-containing fibres

Sample	$\langle P_2 \rangle$	$\langle P_4 \rangle$
5XTA-AS	0.73	0.38
5XTA-HT	0.69	0.31
10XTA-AS	0.65	0.27
10XTA-HT	0.63	0.24

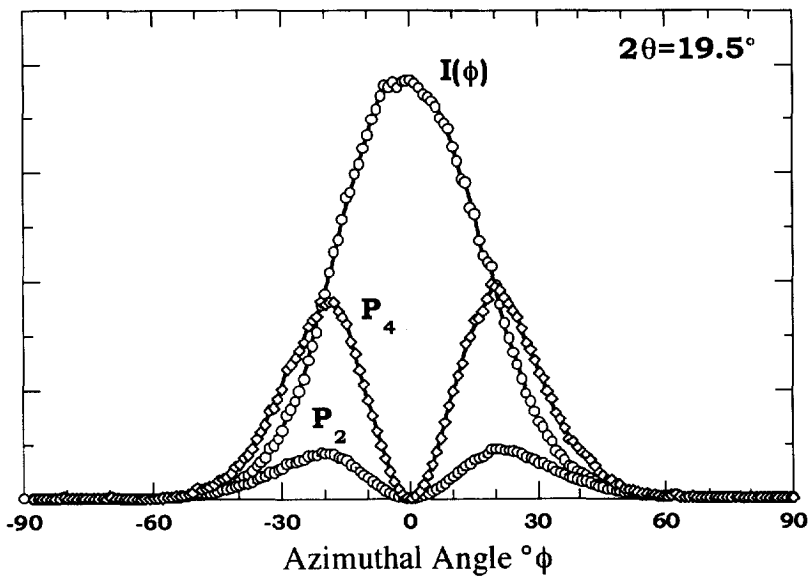

Figure 14 Integrated intensity around the azimuth through the main interchain equatorial peaks at $2\theta = 19.5°$ of the fibre pattern shown in *Figure 13c*. $\phi = -90°$ refers to the fibre (vertical) axis in the pattern. Also plotted are the corresponding Legendre polynomials P2 and P4

angle for the 5XTA fibre prior to heat treatment, where the associated P_2 and P_4 functions are also plotted. *Table 2* summarizes the rather modest order parameter values for all fibres. As expected, the 5XTA fibre displays a higher degree of orientation than the 10XTA fibre; however, the degree of orientation in the heat treated fibres is slightly reduced with respect to their as-spun counterparts, this reduction of orientation likely arising from crystallization of an initially weakly-ordered microstructure.

CONCLUSIONS

1. HBA/HNA-*co*-XTA copolymers with systematic variations in XTA content were synthesized and characterized.
2. There is a processing window above the softening temperature ($\simeq$ 200–250°C) but below the crosslinking reaction temperature ($\simeq$ 350–375°C) within which the polymers exhibit a viscosity minimum and can be melt-processed.
3. When held at elevated temperature, the polymers exhibit an increase in viscosity with time, consistent with the formation of BCB crosslinks, and the extent of solvent swelling decreases and becomes reversible. The swelling behaviour following crosslinking can be used to estimate the degree of crosslinking.
4. The addition of XTA causes a decrease of thermal degradation onset temperature, but virtually no change in char yield at 900°C. The char yields are approximately 40% for all of the materials tested.
5. The addition of XTA units to the HBA/HNA polymer backbone makes it possible to explore the ordered microstructure of the copolymers in more detail. Further studies are necessary to refine our model of the thermotropic liquid crystal polymers in the solid-state.
6. The feasibility of spinning fibres from the HBA/HNA-*co*-XTA copolymers has been confirmed. Further work is necessary to optimize processing conditions. The melt processing of the thermally crosslinkable copolyesters requires stringent temperature control and efficient use of material in order to avoid curing in the spinning chamber or extruder.

REFERENCES

1. Walker, K. A., Markoski, L. J. and Moore, J. S., *Synthesis-Stuttgart*, 1992, **12**, 1265.
2. Jiang, T., Rigney, J., Jones, M. C. G., Markoski, J., Spilman, G. E., Mielewski, D. F. and Martin, D. C., *Macromolecules*, 1995, **28**, 3301.
3. Jones, M.-C., Jiang, T. and Martin, D. C., *Macromolecules*, 1995, **27**, 6507.
4. Calundann, G. W. US Patent No. 4161470, 1979.
5. Charbonneau, L. F. US Patent No. 4429105, 1984.
6. Viney, C., Donald, A. M. and Windle, A. H., *J. Mater. Sci.*, 1983, **18**, 1136.
7. Windle, A. H., Viney, C., Golombok, R., Donald, A. M. and Mitchell, G. R., *Faraday Disc. Chem. Soc.*, 1985, **79**, 55.
8. Gutierrez, G. A., Chivers, R. A., Blackwell, J., Stamatoff, J. B. and Yoon, H., *Polymer*, 1983, **24**, 937.
9. Cheng, S. Z. D., Janimak, J. J., Zhang, A. and Zhou, Z., *Macromolecules*, 1989, **22**, 4240.
10. Sawyer, L. C., Chen, R. T., Jamieson, M. G., Musselman, I. H. and Russell, P. E., *J. Mater. Sci.*, 1993, **28**, 225.
11. Flores, A., Ania, F. and Balta-Calleja, F. J., *Polymer*, 1993, **34**, 2915.
12. Hanna, S., Romo-Uribe, A. and Windle, A. H., *Nature*, 1993, **366**, 546.
13. Wissbrun, K. F., *J. Rheol.*, 1981, **25**, 619.
14. Kalika, D. S., Giles, D. W. and Denn, M. M., *J. Rheol.*, 1990, **34**, 139.
15. Wunder, S. L., Ramachandran, S., Gochanour, C. R. and Weinberg, M., *Macromolecules*, 1986, **19**, 1696.
16. Driscoll, P., Masuda, T. and Fujiwara, K.-I., *Macromolecules*, 1991, **24**, 1567.
17. Kim, S. S. and Han, C. D., *J. Rheol.*, 1993, **37**, 847.
18. Alt, D. J., Hudson, S. D., Garay, R. O. and Fujishiro, K., *Macromolecules*, 1995, **28**, 1575.
19. Romo-Uribe, A. and Windle, A. H., *Macromolecules*, 1993, **26**, 7100.
20. Romo-Uribe, A. and Windle, A. H., *Macromolecules*, 1995, **28**, 7085.
21. Wu, J. L. and Stupp, S. I., *J. Polym. Sci., A*, 1994, **32**, 285.
22. Potter, C. W., Lim, J. C., Serpe, G. and Economy, J., *Prog. Pacific Polym. Sci.*, 1994, **3**, 271.
23. Weinkauf, D. H. and Paul, D. R., *J. Polym. Sci., Part B, Polym. Phys.*, 1992, **30**, 817.
24. Lee, W.-C., DiBenedetto, A. T., Nobile, M. R. and Arcierno, D., *Polym. Eng. Sci.*, 1993, **33**, 156.
25. Barclay, G. C., Ober, C. K., Papathomas, K. I. and Wang, D. W., *J. Poly Sci., Part A, Polym. Chem.*, 1992, **30**, 1831.
26. Barclay, G. C., McNamee, S. G., Ober, C. K., Papathomas, K. I. and Wang, D. W., *J. Polym. Sci., Part A, Polym. Chem.*, 1992, **30**, 1845.
27. Mallon, J. J. and Adams, P. M., *J. Polym. Sci., Part A, Polym. Chem.*, 1993, **31**, 2249.
28. Barklay, G. G. and Ober, C. K., *Prog. Polym. Sci.*, 1993, **18**, 899.
29. Markoski, L. J., Walker, K. A., Deeter, G. A., Spilman, G. E., Martin, D. C. and Moore, J. S., *Chem. Mater.*, 1993, **5**, 248.
30. Dang, T. D., Wang, C. S., Click, W. E., Martin, D. C., Deeter, G. A., Moore, J. S., Husband, D. M. and Arnold, F. E., *Polym. Preprints (Am. Chem. Soc., Div. Polym. Chem.)*, 1995, **36**, 455.
31. Martin, S., unpublished results, 1995.
32. Jiang, T., Spilman, G. E., Martin, D. C., Mather, P. T. and Chaffee, K. P., *Polym. Preprints (Am. Chem. Soc., Div. Polym. Chem.)*, 1996, **37**, 52.
33. Haase, W., Fan, Z. X. and Müller, H. J., *J. Chem. Phys.*, 1988, **89**, 3317.
34. Hanna, S., Windle, A. H., *Polym. Comm.*, 1988, **29**, 237.
35. Kléman, M., in *Liquid Crystallinity in Polymers*, ed. A. Ciferri. VCH, New York, 1991, Ch. 10.
36. Calundann, G. W. and Jaffe, M., *The Robert A. Welch Foundation Conferences on Chemical Research XXVI Synth. Polym.*, Houston, TX, 1982.
37. DeRosa, M. and Winter, H. H., *Rheol. Acta*, 1994, **33**, 220.
38. Bidstrup, S. A., Macosko, C. W., *J. Polym. Sci., Part B, Polym. Phys.*, 1990, **28**, 691.
39. Deeter, G. A., Venkataraman, D., Kampf, J. W. and Moore, J. S., *Macromolecules*, 1994, **27**, 2647.
40. Kirkhoff, R. A., Carriere, C. J., Bruza, K. J., Rondan, N. G., and Sammler, R. L., *J. Macromol. Sci.-Chem.*, 1991, **28**, 1079.
41. Onogi, S. and Asada, T., in *Rheology*, ed. G. Astarita, G. Marrucci and L. Nicolais. Plenum, New York, 1980, pp. 127–147.
42. Larson, R. G. and Doi, M., *J. Rheol.*, 1991, **35**, 539.